Stochastic Geometry-based Analysis of the Impact of Underlying Uncorrelated IoT Networks on LoRa Coverage

Romain Chevillon, Guillaume Andrieux, Laurent Clavier, Jean-François Diouris

IEEE Access
Multidisciplinary | Rapid Review | Open Access Journal

Received November 29, 2021, accepted December 20, 2021, date of publication January 7, 2022, date of current version January 25, 2022.

Digital Object Identifier 10.1109/ACCESS.2022.3141540

Stochastic Geometry-Based Analysis of the Impact of Underlying Uncorrelated IoT Networks on LoRa Coverage

ROMAIN CHEVILLON[1], GUILLAUME ANDRIEUX[1], LAURENT CLAVIER[2], (Senior Member, IEEE), AND JEAN-FRANÇOIS DIOURIS[1]

[1]Nantes Université, CNRS, IETR UMR 6164, F-85000 La Roche-sur-Yon, France
[2]IMT Lille Douai, Institut Mines Télécom, Univ. Lille, CNRS, UMR 8520 - IEMN, F-59000 Lille, France

Corresponding author: Romain Chevillon (romain.chevillon@univ-nantes.fr)

ABSTRACT IoT networks are more and more present nowadays. Some IoT protocols share the same bandwidth leading to interference on neighboring networks and decrease of overall coverage. To contribute to this problem, an analytical study of the coverage of a LoRa network with underlying uncoordinated IoT networks for uplink transmissions is presented in this paper. Using stochastic geometry, closed form analytical expressions are proposed allowing to analyze the success and coverage probabilities for a LoRa network. An appropriate model of the path loss including real-life values is used to characterize the log-distance propagation parameters. The interference comes from both the LoRa network itself and the underlying IoT networks, modeled with an α-stable distribution based on recent measurements. It is shown that for an environment with a huge amount of surrounding uncoordinated IoT networks, the gateways deployment should be doubled to reach a decent coverage probability, compared to an environment where the underlying interfering networks are not considered.

INDEX TERMS LoRa, LPWAN, stochastic geometry, IoT, interference, alpha-stable distributions, coverage.

I. INTRODUCTION

The importance of Internet of Things (IoT) in today's wireless communications systems is increasing day after day. Indeed, many applications related to these new types of Machine-to-Machine (M2M) communications are implemented and integrated in our everyday life: temperature monitoring at given locations in a city [1], waste management [2], smart city usages [3] such as public surveillance, intelligent traffic management [4], [5], smart building monitoring [6], [7], or intelligent healthcare control [8]. With the environmental and health issues that have emerged over the past few years, IoT is quickly becoming a cornerstone of our well-being.

It is estimated by CISCO that more than 500 billion devices will be part of IoT networks by 2030 [9]. Several protocols that are classified according to their ranges have emerged in recent years. First of all, for short radii, so called WPAN for Wireless Personnal Area Networks, protocols like ZigBee [10] or z-Wave [11] have a range of a few dozens of meters. Other protocols classified in the WLAN (for Wireless Local Area Networks) category have longer areas from one to a few kilometers, such as 802.11ah [12]. Finally, protocols like LoRa [13] or SigFox [14] have a range that reaches ten kilometers, and are classified in the Low Power Wide Area Networks category (LPWAN). All these protocols use unlicensed bands (or ISM bands), with a carrier frequency of 868 MHz in Europe and 915 MHz in North America.

Cohabitation between these different networks that share the same frequency bands creates interference on the signals received by the gateways, despite the fact that the modulations for each protocol are different. Therefore, in this paper, we propose to analyze the impact of underlying uncoordinated IoT networks on a LoRa network.

A. RELATED WORKS

Many works about Internet of Things [15], and more especially LoRa communications, emerged a few years ago. In the following of this section, we sort the related works dealing with the three main topics involved in our works:

- LoRa networks modeling,
- path-loss modeling and
- interferential networks identification and modeling.

The associate editor coordinating the review of this manuscript and approving it for publication was Rupak Kharel.

1) LoRa NETWORKS MODELING

Different means to model a network are possible. In this work, we propose to use stochastic geometry [16]. In [17], the authors use a Poisson rain (that is a space-time Poisson process of packets) to model a LoRa network, and analyze the successful reception probability versus the node density for all the spreading factors. The authors in [18] model a unique LoRa cell with end devices (EDs) that are uniformly distributed within a circular area. In [19], the authors model the LoRa network with Poisson Cluster Process (PCP). They calculate theoretically the intra- and inter-cluster interference, and analyze both the coverage probability and the energy efficiency for various values of LoRa nodes and cluster radii. The coverage probability is also calculated using stochastic geometry in [20]. A similar model where both the EDs and the gateways (GWs) are deployed uniformly with homogeneous Poisson-Point Processes (PPPs) is applied by the authors in [21] to optimize the coverage probability of a LoRa network with dual hops. The authors in [22] consider one LoRa cell and use the LoRaWAN capacity model given in [23] to calculate the Packet Delivery Ratio (PDR) for an inhomogeneous distribution of EDs around one gateway. In [24], the authors provide closed-form expressions of coverage probability and area spectral efficiency for a LoRa network with one gateway. Finally, in [25], the success probability and the coverage probability of a LoRa network are calculated litterally and analyzed with the help of stochastic geometry. The results are given versus the densities of GWs and EDs. This work is a good starting point of the present work, even if it takes into consideration a few approximations that are specified in the following sections.

2) PATH LOSS MODELS

Modeling the path-loss for LoRa communications is of crucial interest. Indeed, the path-loss conditions the RSSI of a signal, and therefore the spreading factor that is used. In this context, the authors in [26] evaluate the accuracy of RSSI for different LoRa devices under laboratory conditions, and during a measurement campaign in a semi-urban area. Their results lead to a first path-loss model. The works presented in [27] show the inaccuracy of the parameters of the path-loss models for a relatively dense environment (in Dortmund) for 433 and 868 MHz bands. Various measurements allow the characterization of a new path-loss model that is very close to the observed reality. The modeling is mainly based on the determination of the path-loss exponent (denoted η) and the intercept path-loss. In [28], the authors draw on the work cited above in order to propose path-loss models in the case of rural and urban settings in Lebanon. These models are very accurate for distances of up to 8 km in an urban environment, and 45 km in a rural environment. In [29], the authors propose path-loss models in urban, forest and coastal environments. Finally, the authors in [30] propose to perform similar methods in order to characterize the path-loss for indoor environments.

3) INTERFERENCE IDENTIFICATION AND MODELS

For this paper, the interference coming from neighboring uncoordinated non-LoRa networks must be characterized. In a few works, the authors analyze theoretically and experimentally the interference on a LoRa network, in the case of one gateway. In [31], the authors show the impact of a IEEE 802.15.4g interfering device on a LoRa link, and vice-versa. It is shown that both links have some resilience to interference. In [32], the authors propose two optimization algorithms to determine the best LoRaWAN configurations given an underlying interfering network (here IEEE 802.15.4G). The model that is used in this paper takes into account only one gateway.

In our work, we aim to characterize the underlying IoT networks on a global network, in a multiple gateway scenario, whatever the underlying networks. Recently, this characterization has been the subject of several studies. The packets sent by IoT devices are very short compared to common cellular communications. Then, the noise induced by the underlying IoT networks (e.g. SigFox, 802.11ah, LoRa) can be seen as impulsive [33]. The power and the amplitude of such interference are considered as heavy-tailed random variables, and can be modeled by α-stable distributions [33]. The authors in [33] show that the modeling of interference in IoT networks by α-stable distributions is still valid by adapting the characteristic exponent of the distribution, even when we introduce a guard zone around the receiver and when we limit the power to a finite value. This validation is carried out by comparing the quantiles between the theoretical model and the empirical model. Finally, the works exposed in [34] show a very strong match between the theoretical interference model that is based on an α-stable heavy-tailed distribution and the measurements carried out in different zones (park, hospital, residential and industrial zones) in the city of Aalborg. In view of these related works, α-stable distribution is a good choice to model the interference from the underlying networks.

B. CONTRIBUTIONS AND ORGANIZATION

As seen in the previous sections, the related works that deal with LoRa networks modeling mainly focus on co-SF interference to calculate the coverage probability. These works do not take into account the uncoordinated neighboring networks, and do not model the path-loss with real parameters. Note that the premises of the studies presented in this article were introduced in [35]. The present paper proposes an improved and more complete system model than the one included in [35], and more thorough results and analysis.

In this paper, a LoRa network in an uplink configuration that considers various end devices densities and gateways densities is introduced. This system permits to model both dense and sparse networks. Then, the main contributions of this work are as follows:

- The presence of all possible underlying IoT networks (e.g. SigFox, 802.11ah, LoRa) concurrently to the

considered LoRa network is taken into account for a coverage probability calculation in a multiple gateway scenario. The interference induced by these uncoordinated networks are modeled by a heavy-tailed distribution. The parameters of the α-stable distribution are obtained by in-situ measurements and have been validated in [33], [34]. This model has been shown to fit the data.
- The path-loss used for all the communications is modeled by a regression curve that aggregates real-life path-loss exponent and intercept. Indeed, most stochastic geometry-based papers dealing with LoRa networks usually consider common path-loss model. The contribution of our approach lies in the use of such a more realistic path-loss model with experimental data proven and validated in [27] in order to get as close as possible to the experimental values of path loss for LoRa links at 868 MHz.
- The coverage probability for this LoRa network with the improved path-loss model and the α-stable distributed uncoordinated networks interference is given for various values of ED and GW densities. Note that the analytical results for one gateway have been validated by numerical simulations in [25], and the system model with multiple gateways based on stochastic geometry calculations was compared and validated with simulations in our previous works [16], [36].
- The values of the SF-based ED densities are not obtained with analytical approximations (as made in related works) but with Monte-Carlo simulations that converge to results that are much closer to the true values.

In Section II, we introduce the system model. All the analyzed metrics and the theoretical approach on the interference models are presented in Section III. In Section IV, we depict and discuss the analytical and numerical calculations for SNR, SIR and coverage probability. Finally, conclusions are given in Section V.

II. SYSTEM MODEL

In this section, we introduce the system model through several assumptions. The system includes a LoRa network with another underlying IoT network. Note that for this paper, we focus on the uplink. This system is schematized on Fig. 1. All the notations introduced in this model are given in Table 1.

A. ASSUMPTION 1 (SPATIAL MODEL FOR END DEVICES AND GATEWAYS)

The system models an infinite LoRa network, made up of gateways (GWs) and end devices (EDs) in an infinite $\mathbb{R}^2$ space [37]. The GWs are uniformly and randomly located in the $\mathbb{R}^2$ space, and are modeled by a homogeneous Poisson-Point Process (PPP) Φ_G with intensity λ_G. The EDs are modeled by an independently marked PPP [36] denoted as

$$\tilde{\Phi}_E = \left\{\left(\mathbf{e}_i, \mathcal{P}, d_{ij}, \mathrm{SF}_i\right)\right\}, \tag{1}$$

where $\{\mathbf{e}_i\}$, $\mathcal{P}$, $\left\{d_{ij}\right\}$, and $\{\mathrm{SF}_i\}$ denote the sets of ED locations, the ED transmit power, the length of the LoRa radio links (i.e. the distance between the i-th ED and its receiving j-th GW), and the assigned Spreading Factor (SF). The locations $\mathbf{e}_i$ are determined according to an unmarked PPP $\Phi_E \in \mathbb{R}^2$ with intensity λ_E (with $\lambda_G \ll \lambda_E$). We consider that all EDs transmit with a constant power $\mathcal{P} = 19$ dBm [38].

B. ASSUMPTION 2 (EUCLIDEAN DISTANCES BETWEEN END DEVICES AND GATEWAYS)

Each GW is characterized by its index j (G_j) and its position $\mathbf{g}_j$ on the plane. We consider that G_0 is located at the origin of the coordinate system, i.e. $\mathbf{g}_0 = (0, 0)$. Likewise, each ED is characterized by its index i (E_i) and by its position $\mathbf{e}_i$. Each ED is connected to the closest gateway (as explained by the authors in [37], the distance r to the closest gateway is distributed according to $f_1(r) = 2\pi\lambda_G r e^{\lambda_G \pi r^2}$). Assuming that E_i is connected to G_j, the Euclidean distance (in km) between E_i and G_j is $d_{ij} = \left|\mathbf{e}_i - \mathbf{g}_j\right|$.

C. ASSUMPTION 3 (BASEBAND RECEIVED SIGNAL BY A GATEWAY)

As we focus on the uplink, the GW receives the useful signal, the interference coming from the other LoRa EDs, the aggregate interference coming from the underlying uncoordinated IoT networks, and the Additive White Gaussian Noise [25], [32]. Then, the baseband received signal by G_j can be given by (2), as shown at the bottom of the next page, where $U_j[n]$ denotes the useful signal, $I_j[n]$ the interference created by the other LoRa transmitters from the studied LoRa network, $p(d_{ij})$ the path loss attenuation, $g_{t,i}$ the i-th transmitter ED antenna gain, $g_{r,j}$ the j-th receiver antenna gain, h_{ij} the fast fading coefficient between the i-th transmitter and the j-th receiver, $S_i[n]$ the unit-variance signal sent by the i-th ED, $\ddot{\Phi}_{E_k}$ the set of all the interfering EDs that transmit data at the same time as the i-th ED, $A[n]$ the Additive White Gaussian Noise (AWGN), $Z_j[n]$ the aggregate interference coming from the neighboring non-LoRa networks and $N_j[n]$ the total noise.

D. ASSUMPTION 4 (PATH LOSS ATTENUATION)

In this paper, we assume that the signals sent by the EDs experience a path loss attenuation that is a function of the distance between each ED and the receiving GW. The path loss in dB varies with distance according to the following equation [28], [29]:

$$\mathrm{PL}(d_{ij})[dB] = 10\eta \log_{10}\left(\frac{d_{ij}}{d_0}\right) + \mathrm{PL}_0, \tag{3}$$

where η, d_{ij} and PL_0 denote the path loss exponent, the distance between E_i and G_j in km and the path loss at a reference distance $d_0 = 1$ km, respectively. Then, for a given

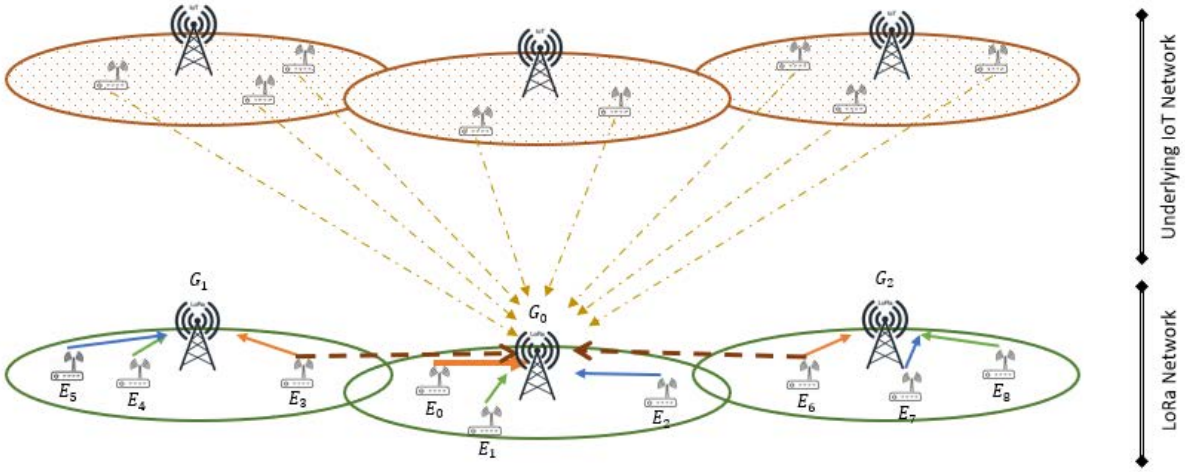

FIGURE 1. Graphical model of the system. The studied LoRa network is depicted in the lower layer of this figure. The ED-GWs communications are represented by solid arrows. The colors of the LoRa links between the EDs and their relative GW correspond to the SFs used for the communications. Note that we take into account the link between E_0 and G_0. The interference induced by the LoRa communications are depicted in dotted lines. On the upper layer of this figure is depicted an underlying IoT network (e.g. Sigfox network). The interference on the studied GW (G_0) coming from this underlying network are depicted as dotted orange lines.

ED i, the path loss attenuation between this ED and the j-th GW is expressed as follows:

$$p(d_{ij}) = 10^{-\frac{\mathrm{PL}_0}{10}} \left(\frac{d_{ij}}{d_0}\right)^{-\eta}. \tag{4}$$

The path loss parameters directly depend on the environment. These parameters are derived from fitting curves over measured data. In our work, we propose to take into account the path loss parameters measured and modeled in the city of Dortmund for LoRa links at 868 MHz, given in [27], i.e. $\eta = 2.65$ and $\mathrm{PL}_0 = 132.25$ dB. Moreover, we assume that both the receiving and the transmitting antennas are isotropic. Consequently, both the receiving and transmitting antennas have a unit gain, i.e. $g_{t,i} = g_{r,j} = 1, \forall(i,j)$ [25].

E. ASSUMPTION 5 (SMALL-SCALE FADING AND AWGN NOISE)

Small-scale fading describes the rapid fluctuations in the amplitude and phase of a signal over a short period of time or a short distance [39]. In this model, the envelope of the received signal is statistically described by a Rayleigh distribution. The small scale fading induced between E_i and G_j denoted as h_{ij} follows a Rayleigh distribution. Then, in terms of power, $\|h_{ij}\|^2 \sim \mathrm{Exp}(1)$.

We assume Additive White Gaussian Noise (AWGN), denoted as $A[n]$ in (2), with zero-mean and power $\mathcal{P}_A = -174 + \mathrm{NF} + 10\log \mathrm{BW}$ dBm, where $\mathrm{NF} = 6$ dB is the receiver noise figure and $\mathrm{BW} = 125$ kHz is the bandwidth of the signal [25].

F. ASSUMPTION 6 (SPREADING FACTOR ALLOCATION)

In the case of LoRa communications, an SF is allocated to each ED according to its distance from the GW to which it is connected [25]. This allocation is typically done by the NetServer which sends feedback in response to short test frames transmitted by the ED after connecting to the network. The SF are between 7 and 12. Tab. 2 and Fig. 2 list the allocations of SF (SF_i) as a function of the distance d_{ij} between an ED (E_i) and its associated GW G_j. For example, if the distance d_{ij} between E_i and its associated gateway G_j is comprised between l_3 and l_4 (i.e. between 3 and 4 km), the SF associated with this ED will be $\mathrm{SF}_i = 10$. This allocation of SF according to the distances EDs-GWs therefore leads to a spatial formation of rings centered on the positions of the GWs, as shown in Fig. 3.

G. ASSUMPTION 7 (NON-LoRa INTERFERING NETWORKS)

We consider that the studied LoRa network is located in a space where other underlying IoT networks using the same European ISM frequency bands (868 MHz) such as Sigfox, z-Wave, 802.11ah or Zigbee coexist. Even though they do not use the same technology, these non-LoRa networks interfere with LoRa communications. As studied in [34], this

$$Y_j[n] = \underbrace{\sqrt{\mathcal{P}p(d_{ij})g_{t,i}g_{r,j}h_{ij}^2}S_i[n]}_{U_j[n]} + \underbrace{\sum_{E_k \in \ddot{\Phi}_{E_k} \setminus E_i} \sqrt{\mathcal{P}p(d_{kj})g_{t,k}g_{r,j}h_{kj}^2}S_k[n]}_{I_j[n]} + \underbrace{A[n] + Z_j[n]}_{N_j[n]}, \tag{2}$$

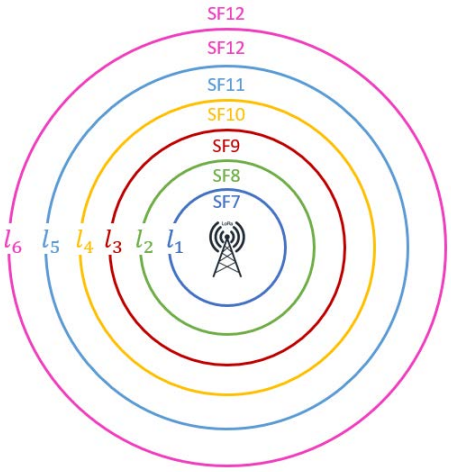

FIGURE 2. Spreading Factor Allocation. The ranges corresponding to SF 7, 8, 9, 10, 11 and 12 (cf. Table 2) are depicted in blue, green, red, yellow, cyan and magenta, respectively.

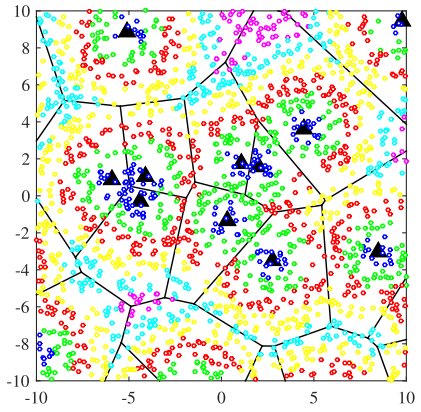

FIGURE 3. Spatial representation of the system model with $\lambda_G = 0.025$ GWs per km^2 and $\lambda_E = 5$ EDs per km^2. The GWs are the black triangles, while the EDs are the points. Each ED are colored according to its SF assignment. EDs in SF 7, 8, 9, 10, 11 and 12 are colored in blue, green, red, yellow, cyan and magenta, respectively. Units on the axis are in km.

interference can be regarded as noise. However, the modeling of this interference by an AWGN is not a good choice. Therefore, we propose to model the interference Z_j by an α-stable noise, the measurement data of [34] indeed suggesting that the distribution of the power of the interference is heavy tailed [40].

It has been shown in [41] and in [34] that network interference are well-modeled by impulsive noise, and more particularly by α-stable noise. The measurement in [34] details a LoRa-like configuration with frequency bands of 125 kHz. The power is shown to be heavy tailed. Considering the α-stable model from [41], conditioned on the set of active interfering devices Φ_α, the interference is Gaussian and its mean power depends on this set Φ_α. Finally, the power, unconditioning on Φ_α, is a totally skewed α-stable random variable, as it has been proven and validated analytically and experimentally in [33], [34]. Note that even if the powers of the LoRa emitters is fixed, the powers of the non-LoRa emitters are random. Then, the use of α-stable distribution to model the interference coming from the underlying uncorrelated IoT networks is valid according to [41].

Thus, in (2), the term Z_j is considered as an interferential noise for the j-th GW, and the power $\mathcal{P}_Z$ of this interferential noise follows an α-stable distribution:

$$\mathcal{P}_Z \sim S_\alpha(\gamma, \beta, \delta), \tag{5}$$

where α, γ, β and δ are the characteristic exponent (with $0 < \alpha < 2$), the scale parameter (with $\gamma \in \mathbb{R}_+$), the skew parameter (with $\beta \in [-1, 1]$) and the shift parameter (with $\delta \in \mathbb{R}$), respectively.

This model is not exactly supported by the data from [34] because the α should be given by the inverse of the channel attenuation (so less than one) but this is generally not the case in the measurement with estimated values ranging from 0.94 in the Hospital complex to 1.77 in the industrial area. However this is consistent with [40] that shows that a more realistic device location gives an interference adequately modeled by an α-stable distribution but with a modified α. In the following we will choose a value of alpha of 1.69 which is obtained for the residential area. Measured dispersion (γ) values are found between 10^{-11} and 10^{-10}. They are expected to increase with the increase in device density as it is shown in the theoretical results from [34]. Consequently we chose a value of 10^{-10} and 2.10^{-10} for a moderately interfering scenario and a denser scenario.

III. STOCHASTIC GEOMETRY METRICS AND INTERFERENCE CHARACTERIZATION

A. PRELIMINARY DEFINITIONS

1) SUCCESS PROBABILITY

In many works dealing with stochastic geometry applied to cellular networks such as [36], the performances are measured from the Signal-to-Interference-plus-Noise-Ratio (SINR). Nevertheless, it is not possible to calculate the coverage probability of a LoRa network with this SINR-based methodology [23].

Thus, in a LoRa network, two conditions must be met to specify the success of a transmission from an ED to a GW:

i) the Signal-to-Noise Ratio (SNR) should be greater than a certain threshold q_{SF_i} depending on the used SF and
ii) the Signal-to-Interference Ratio (SIR) should be greater than a certain threshold w.

Then, the success of the transmission between the i-th ED and the j-th GW can be written as follows [25]:

$$(\mathrm{SNR}_{ij} \geq q_{\mathrm{SF}_i}) \bigcap (\mathrm{SIR}_{ij} \geq w), \tag{6}$$

where SNR_{ij}, SIR_{ij}, q_{SF_i} and w denote the SNR and the SIR of the LoRa link between the i-th ED and the j-th GW, the SNR threshold for the SF used for the communication between E_i and G_j, and the SIR collision threshold between different SF, respectively.

TABLE 1. Notation and simulation parameters.

Symbol	Meaning	Default Value
Φ_G	PPP of GWs, with intensity λ_G	$\lambda_G = 0.005$ GWs per km^2 $\lambda_G = 0.01$ GWs per km^2 $\lambda_G = 0.05$ GWs per km^2
Φ_E	PPP of EDs, with intensity λ_E	$\lambda_E = 5$ EDs per km^2
Φ_{E_k}	PPP of the EDs that use the same SF_k, with intensity λ_{E_k}	
$\ddot{\Phi}_{E_k}$	PPP of the EDs that use the same SF_k and that transmit at the same time slot, with intensity $\ddot{\lambda}_{E_k}$	$\ddot{\lambda}_{E_k} = \xi \cdot \lambda_{E_k}$, with $\xi = 0.01$
$\mathcal{P}$	Transmission power of the EDs	$\mathcal{P} = 19$ dBm
d_{ij}	Distance between the i-th ED and the j-th GW	
h_{ij}	Fading channel between ED i and GW j	$\lvert h_{ij}\rvert^2 \sim \mathrm{Exp}(1)$
η	Path-loss exponent	$\eta = 2.65$ [27]
SF_i	Spreading factor used by the i-th ED	
$g_{t,i}, g_{r,j}$	i-th transmitter ED antenna gain and j-th receiver antenna gain	$g_{t,i} = 1, g_{r,j} = 1$
BW	Bandwidth of the signal	BW $= 125$ kHz
NF	Receiver noise figure	NF $= 6$ dB
λ	Carrier wavelength	$\lambda = 34.5$ cm
PL_0	Path loss at a reference distance $d_0 = 1$ km	$\mathrm{PL}_0 = 132.25$ dB [27]
q_{SF_i}	SNR threshold for the SF used by the i-th ED	cf. Tab. 2
w	SIR threshold	$w = 1$ dB
$\mathcal{P}_A$	AWGN power	$\mathcal{W} = -174 + \mathrm{NF} + 10 \log \mathrm{BW}$ [dBm]
l_k	Inferior boundary for SF_{k+7}	$l_k = k$ kilometers
$\mathrm{H}(\mathbf{e}_i)$	Success probability metric for the i-th ED	
$\mathcal{L}_{I_j}(x)$	Laplace transform of the random variable I_j at x	
$\mathcal{Z} \sim S_\alpha(\gamma, \beta, \delta)$	Random variable $\mathcal{Z}$ following an α-stable distribution with characteristic exponent α, scale parameter γ, skew parameter β and shift parameter δ	$\alpha = 1.69, \beta = 1, \delta = 0$, [34] $\gamma_1 = 1 \cdot 10^{-10}$, $\gamma_2 = 2 \cdot 10^{-10}$
$\mathcal{C}$	Coverage probability	-

Obviously, the success of a transmission depends on the distance between the transmitter ED and the receiver GW. We introduce the success probability metric that is depicted as follows [25]:

$$\mathrm{H}(\mathbf{e}_i) = \mathbb{P}\left[\bigcup_j \{(\mathrm{SNR}_{ij} \geq q_{\mathrm{SF}_i}) \bigcap (\mathrm{SIR}_{ij} \geq w)\}\right], \quad (7)$$

which means that both conditions on the SNR and the SIR for the i-th ED are met with at least one GW. Thus, the success probability corresponds to the probability that an ED can be connected to at least one GW.

2) COVERAGE PROBABILITY

As seen in the previous section, the success probability of a transmission is linked to the distance between the transmitting ED and the receiving GW. Recall that the coverage probability is the probability that a random element of the transmitters is not in outage, at any chosen time. Thus, the coverage probability can be expressed as follows [25]:

$$\mathcal{C} = \int_{\mathbb{R}_+} \mathrm{H}(\mathbf{e}_i) f_d(d_{ij}) \mathrm{d}d_{ij}, \quad (8)$$

where $f_d(x) = 2\pi\lambda_G x e^{-\lambda_G \pi x^2}$ is the distance distribution of a random ED to its nearest GW.

B. SIGNAL-TO-NOISE RATIO (SNR)

As we have seen in the previous section, the calculation of the coverage probability is possible only if we retrieve the SNR and SIR. Thus, it is necessary to characterize both the interference and the noise implied in each LoRa communication, i.e. the powers of the elements $I_j[n]$ and $N_j[n]$ in (2). As shown previously and on Fig. 1, the interference come from both the LoRa EDs and the non-LoRa EDs.

1) TOTAL NOISE

In our work, we propose to incorporate this interferential noise Z_j with an α-stable distributed power $\mathcal{P}_Z$ in the total noise N_j with a power $\mathcal{P}_N$. As seen in the previous sections, the total noise also includes the AWGN A, with a power $\mathcal{P}_A$. We consider that AWGN and interferential noise are strictly independent. The total noise power can be expressed as:

$$\mathcal{P}_N = \mathcal{P}_A + \mathcal{P}_Z. \quad (9)$$

2) SNR SUCCESS PROBABILITY

As explained previously, the SNR can be expressed as follows:

$$\mathrm{SNR}_{ij} = \frac{\mathcal{P}p(d_{ij}) g_{t,i} g_{r,j} |h_{ij}|^2}{\mathcal{P}_N} = \frac{\mathcal{P}p(d_{ij}) |h_{ij}|^2}{\mathcal{P}_A + \mathcal{P}_Z}. \quad (10)$$

The success probability relative to the SNR directly depends on a SF-based threshold q_{SF} which are given in Tab. 2.

The success probability relative to the SNR corresponds to the probability that the SNR is greater than or equal to the threshold (for a given SF). Then,

$$\mathbb{P}\left[\mathrm{SNR}_{ij} \geq q_{\mathrm{SF}_i}\right] = \mathbb{P}\left[|h_{ij}|^2 \geq \frac{(\mathcal{P}_A + \mathcal{P}_Z)\, q_{\mathrm{SF}_i}}{\mathcal{P}p(d_{ij})}\right]$$

TABLE 2. SNR thresholds.

SF	bit-rate kb/s	Packet air-time ms	Tx /h	Receiver Sens.	SNR q_{SF} dB	Range km
7	5.47	36.6	98	-123 dBm	-6	$l_0 - l_1$
8	3.13	64	56	-126	-9	$l_1 - l_2$
9	1.76	113	31	-129	-12	$l_2 - l_3$
10	0.98	204	17	-132	-15	$l_3 - l_4$
11	0.54	372	9	-134.5	-17.5	$l_4 - l_5$
12	0.29	682	5	-137	-20	$> l_5$

$$= \mathbb{E}\left[e^{-\frac{(\mathcal{P}_A+\mathcal{P}_Z)q_{\mathrm{SF}_i}}{\mathcal{P}p(d_{ij})}}\right]$$
$$= e^{-\frac{\mathcal{P}_A q_{\mathrm{SF}_i}}{\mathcal{P}p(d_{ij})}}\mathbb{E}\left[e^{-\frac{\mathcal{P}_Z q_{\mathrm{SF}_i}}{\mathcal{P}p(d_{ij})}}\right]$$
$$= e^{-\frac{\mathcal{P}_A q_{\mathrm{SF}_i}}{\mathcal{P}p(d_{ij})}}\exp\left[-\frac{\gamma^\alpha}{\cos\frac{\pi\alpha}{2}}\left(\frac{q_{SF_i}}{\mathcal{P}p(d_{ij})}\right)^\alpha\right]. \quad (11)$$

The first equality comes from the characterization of the SNR in Section III-B2, the second equality comes from the fact that $h_{ij}^2 \sim \mathrm{Exp}(1)$, the third equality comes from the independance between the AWGN noise $\mathcal{P}_A$ and the interferential noise $\mathcal{P}_Z$. In [34], it is proven that the β parameter of the α-stable distribution equals 1. This assumption leads us to the fourth equality that comes from the definition of the Laplace transform of a random variable that follows an α-stable distribution with $\beta = 1$ [42].

C. SIGNAL-TO-INTERFERENCE RATIO (SIR)

1) LoRa INTERFERENCE CHARACTERIZATION

As depicted on Fig. 1 and in (2), the interference taken into account for the calculation of the SIR come from the LoRa EDs that transmit their data in the same time interval as the considered link. In this section, we propose to characterize these interference $I_j[n]$, and their relative power $\mathcal{I}_j$.

LoRa technologies enable the reception of signals from numerous EDs thanks to the orthogonality of the transmission subbands and the quasi-orthogonality of SFs. Despite the fact that some works such as [43] and [44] show that the imperfect orthogonality between each concurrent SFs results to a further coverage loss, we propose to take into account the co-SF interference (i.e. the interference coming from the EDs that use the same SF). Indeed, the practical rejection gain between quasi-orthogonal SFs ranges from 16 to 36 dB [25], which is quite high for our purpose.

We consider Φ_E the set of the EDs in $\mathbb{R}$. This set is formed thanks to a PPP with density λ_E. In order to characterize the interference on a typical link, it is necessary to identify the set of the interferers:

- the set of the EDs that use the same typical link SF (Φ_{E_k} with density λ_{E_k}),
- the set of the EDs that both use the same SF and transmit at the same time slot ($\ddot{\Phi}_{E_k}$ with density $\ddot{\lambda}_{E_k}$).

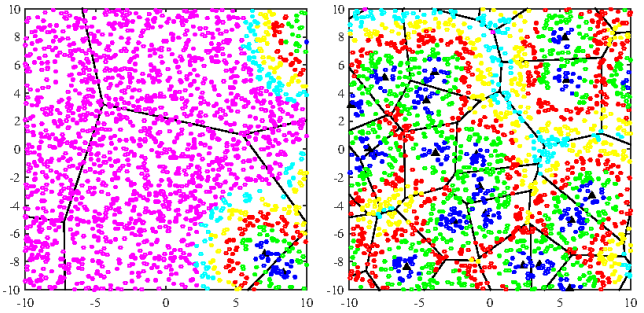

FIGURE 4. Spatial representation of the system model for a sparse ($\lambda_G = 0.005$ GWs per km^2) and a dense ($\lambda_G = 0.05$ GWs per km^2) gateway deployment. The EDs are colored the same way as in Fig. 3. Units on the axis are in km.

The duty cycle policy enforced by ETSI for LoRaWAN communications is set to $\xi = 1\%$ [13]. Then, the density of the EDs that transmit at the same time slot is $\ddot{\lambda}_{E_k} = \xi\lambda_{E_k}$.

As the density of the effective interferers directly depends on the intensity of the EDs that use the same SF, we propose to characterize the density λ_{E_k}.

a: CHARACTERIZATION OF λ_{E_k}

The PPP of the EDs Φ_E can be divided into six PPPs Φ_{E_k}, with $k \in [7, 12]$ that correspond to the PPP of all the EDs that use the same SF. For instance, if E_i belongs to $\Phi_{E_{11}}$, it means that E_i transmits its data with SF 11. According to Tab. 2, it also means that it is located between l_4 and l_5 km away from its related GW.

Nevertheless, the calculation of the densities λ_{E_k} is not so simple. Indeed, as shown in Fig. 4, these densities depend on the density of the GW deployment. For sparse GW deployment ($\lambda_G = 0.005$ GWs per km^2), the number of EDs that use SF 12 is prominent (i.e. $\lambda_{E_{12}}$), as shown on the left plot of Fig. 4. This is due to the fact that the distances between the GWs are large, and thus, most of the EDs are also very far from their related GW. In the contrary case, for a dense GW deployment ($\lambda_G = 0.05$ GWs per km^2), the GWs are very close. As the EDs are linked to their nearest GW, this leads to the fact that most of the EDs use low SFs as shown on the right plot of Fig. 4.

In [25], the authors propose a theoretical approximation of the densities λ_{E_k} in both sparse and dense GW deployment. For sparse GW deployment (i.e. when $\lambda_G \ll 1$), the densities of the EDs for each SF are given by:

$$\lambda_{E_k} \approx \begin{cases} \lambda_G\lambda_E\pi\left(l_{k-6}^2 - l_{k-7}^2\right), & \forall k \in [7, 11] \\ \lambda_E - \sum_{i=7}^{11}\lambda_{E_i}, & k = 12, \end{cases} \quad (12)$$

and for dense GW deployment, these densities are approximated as follows:

$$\lambda_{E_k} \approx \begin{cases} \lambda_G\lambda_E\pi\left(l_{k-6}^2 - l_{k-7}^2\right)e^{\pi v_k\lambda_G}, & \forall k \in [7, 11] \\ \lambda_E - \sum_{i=7}^{11}\lambda_{E_i}, & k = 12, \end{cases} \quad (13)$$

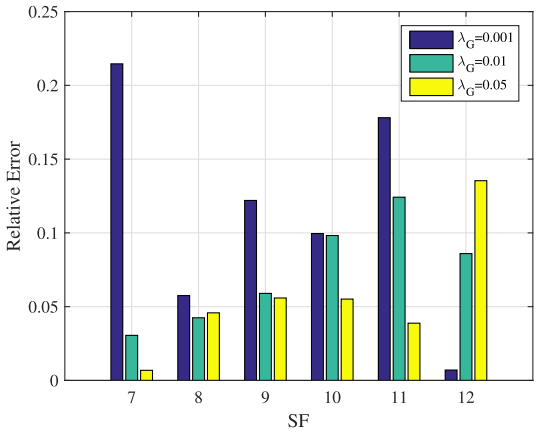

FIGURE 5. Relative error between simulated and approximated EDs densities for SFs 7 to 12, with $\lambda_E = 5$ EDs per km^2. λ_G is given in GWs per km^2.

where v_k are the fitting parameters for SF_k defined in [25]. In order to characterize more deeply the interfering devices sets, we propose to

i) identify practically the densities of the different SF-based interfering sets,
ii) evaluate the relative error between the simulated densities and the approximated ones taken from [25], and
iii) choose between both methods (simulated or approximated) for the theoretical calculations.

b: SF-BASED EDs DENSITIES IDENTIFICATION

We identify the densities for the different SF-based EDs sets using Monte-Carlo simulations. For this purpose, λ_E is set to 5 EDs per km^2. The values of the GW densities vary between $\lambda_G = 0.001$ GWs per km^2 (i.e. sparse GW deployment) and $\lambda_G = 0.1$ GWs per km^2 (i.e. dense GW deployment) and the densities λ_{E_k} are calculated in a 40.000 km^2 space. The convergence of the densities values is reached after 3.500 Monte-Carlo rounds. The results of the various SF-based densities λ_{E_k} are given in Tab. 3.

Fig. 5 shows the relative error between the simulated ED densities for all the SFs depicted in Tab. 3 and the approximated values taken from (12) and (13). This figure clearly shows the limits of the approximations. Indeed, for SFs 8, 9 and 10, the error reaches a maximum error rate of 12% for all the GW deployment densities. Nevertheless, the error rate for SF7 is higher (21%) in the case of a very sparse GW deployment ($\lambda_G = 0.001$), which is mainly due to the huge density of the SF12 EDs (as seen in the left plot of Fig. 4). On the other hand, for dense GW deployment, the error rate is quite high for SF11 and SF12, which is linked to the fact that the density of low SFs is very high in these cases, as shown in the right plot of Fig. 4.

In the following of this paper, we propose to use the values of λ_{E_k} given in Tab. 3 that are better than the ones given in [25] to calculate the related densities $\ddot{\lambda}_{E_k}$.

2) SIR SUCCESS PROBABILITY

Thanks to the previous results on the interference characterization, the SIR can be expressed as follows:

$$\mathrm{SIR}_{ij} = \frac{\mathcal{P}p(d_{ij})g_{t,i}g_{r,j}|h_{ij}|^2}{\mathcal{I}_j} \tag{14}$$

$$= \frac{\mathcal{P}p(d_{ij})|h_{ij}|^2}{\sum_{E_k \in \ddot{\Phi}_{E_k} \setminus E_i} \mathcal{P}p(d_{kj})h_{kj}^2}. \tag{15}$$

The success probability relative to the SIR directly depends on a SF-based collisions threshold. In our works, as we only take into account the co-SF interference, we assume that the required aggregate SIR for a successful transmission is set to $w = 1$ dB, so $w = 1.259$ [43].

Proposition 1: The success probability relative to the SIR is:

$$\mathbb{P}[\mathrm{SIR}_{ij} \geq w] = \mathcal{L}_{\mathcal{I}_j}\left(\frac{w}{\mathcal{P}p(d_{ij})}\right), \tag{16}$$

where $\mathcal{L}_{\mathcal{I}_j}\left(\frac{w}{\mathcal{P}p(d_{ij})}\right)$ is the Laplace transform of the random variable $\mathcal{I}_j$ at $\frac{w}{\mathcal{P}p(d_{ij})}$ conditioned on the locations of the ED at $\mathbf{e}_i$ and the GW at $\mathbf{g}_j$, and

$$\mathcal{L}_{\mathcal{I}_j}\left(\frac{w}{\mathcal{P}p(d_{ij})}\right) = \exp\left(-\frac{2\pi\ddot{\lambda}_{E_k} w d_{ij}^{\eta}}{l_{k-7}^{\eta-2}(\eta-2)}\mathrm{GHF}\left(\frac{wd_{ij}}{l_{k-7}^{\eta}}\right)\right), \tag{17}$$

where GHF (x) is the Gauss Hypergeometric function defined as $\mathrm{GHF}(x) = {}_2F_1\left(1, 1-\frac{2}{\eta}, 2-\frac{2}{\eta}, -x\right)$.

Proof: See Appendix A. ∎

D. SUCCESS AND COVERAGE PROBABILITIES

Proposition 2: For a given E_i that is effectively connected to G_0, the success probability of the transmission is given in (18), as shown at the bottom of the next page.

Proof: See Appendix B. ∎

Finally, the coverage probability is calculated with (8). Note that the coverage probability has no closed form, and is calculated numerically.

IV. NUMERICAL ANALYSIS

In this section, the stochastic geometry metrics are presented through analytical results obtained from the equations given in Section III. For more clarity, we assume that E_i is connected to G_0 that is located at the origin of the plane.

A. SNR SUCCESS PROBABILITY ANALYSIS

We can see in (11) that the SNR success probability (denoted as $\mathbb{P}\left[\mathrm{SNR}_{ij} \geq q_{\mathrm{SF}_i}\right]$) depends on the distance between the EDs and their GW (i.e. the SF that they use for the transmission), and the interferential noise power. Fig. 6 shows the Signal-to-Noise Ratio success probability for AWGN-only noise (blue curve) and for AWGN plus interferential α-stable noise (red and green curves) vs. distance d_{i0} between the i-th ED and its relative 0-th GW. The α-stable noise is modeled with the values given in Tab. 1. The red curve describes the behavior of the SNR success probability in a sub-urban

TABLE 3. Practical λ_{E_k} densities with $\lambda_E = 5$ EDs per km^2.

λ_{E_k}	$\lambda_G = 0.001$	$\lambda_G = 0.005$	$\lambda_G = 0.01$	$\lambda_G = 0.025$	$\lambda_G = 0.05$	$\lambda_G = 0.1$
λ_{E_7}	0.02	0.08	0.15	0.37	0.72	1.33
λ_{E_8}	0.05	0.22	0.42	0.94	1.56	2.17
λ_{E_9}	0.07	0.33	0.61	1.13	1.40	1.13
$\lambda_{E_{10}}$	0.10	0.41	0.69	0.99	0.81	0.30
$\lambda_{E_{11}}$	0.12	0.45	0.68	0.71	0.34	0.05
$\lambda_{E_{12}}$	4.64	3.50	2.45	0.87	0.17	0.01

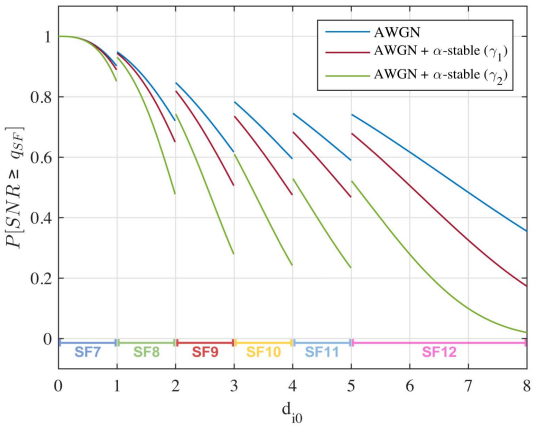

FIGURE 6. Signal-to-Noise Ratio success probability for AWGN-only noise (blue curve) and for AWGN plus interferential α-stable noise vs. distance d_{i0} in km.

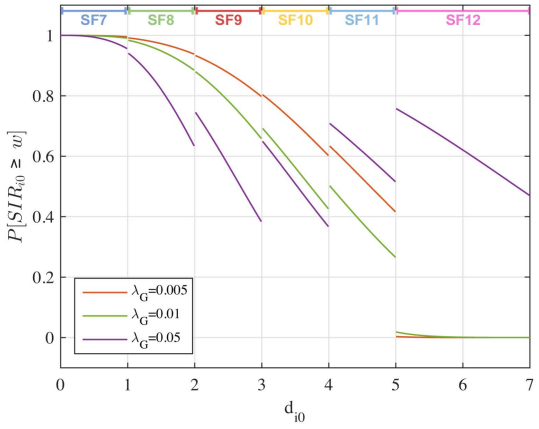

FIGURE 7. Signal-to-Interference Ratio success probability vs. distance d_{i0} in km. λ_G is given in GWs per km^2.

environment (i.e. for $\gamma = \gamma_1 = 1 \cdot 10^{-10}$) while the green curve stands for an urban environment (i.e. for $\gamma = \gamma_2 = 2 \cdot 10^{-10}$).

First, in all cases, we can see that the curves decrease with the distance d_{i0}. The curves are discontinuous at all l_k step values. These two observations are relatively obvious in view of (11) which takes into account the allocations of SF as a function of the distance from E_i to G_0. It is obvious that the addition of interference decreases the SNR success probability. Indeed, this probability reaches a level of 0.8 for $d_{i0} = 1.7$ km (with SF 8) and $d_{i0} = 2.2$ km (with SF 9) for an environment without α-stable noise, for $d_{i0} = 1.6$ km with α-stable noise with $\gamma = \gamma_1$ and $d_{i0} = 1.4$ km for $\gamma = \gamma_2$. Even more explicitly, the probability is never lower than 0.2 for an environment without α-stable noise, but reaches 0.2 from $d_{i0} = 7.85$ km with an α-stable noise with $\gamma = \gamma_1$ and from $d_{i0} = 6.4$ km for $\gamma = \gamma_2$ (i.e. with SF 12). Despite the fact that the α-stable signal strength with γ_2 is only twice as strong as that with γ_1, the SNR success probability is drastically reduced. It can therefore be concluded that the presence of many underlying IoT networks can lead to a very strong decrease in SNR, and therefore a decrease in the SNR success probability, even for very short ED-GW distances. In an very dense urban environment (in terms of IoT networks), this drastic decrease in the SNR success probability will inevitably decrease the overall coverage probability for the studied LoRa network.

B. SIR ANALYSIS

Fig. 7 shows the Signal-to-Interference Ratio success probability vs. distance $d = d_{i0}$ between the i-th ED and its relative 0-th GW. The curves are obtained thanks to (16), for $\lambda_E = 5$ EDs per km^2 and $\lambda_G = 0.005, 0.01, 0.05$ (orange curve, green curve and purple curves, respectively) GWs per km^2.

Like the SNR, the SIR is decreasing as a function of d_{i0} for all the values of λ_G, in a discontinuous way. This discontinuity is due to the different SIR thresholds for all the SFs. We clearly see that for a sparse network (i.e. $\lambda_G = 0.005$), the SIR coverage probability is almost continuously decreasing

$$\mathrm{H}(d_{i0}) = 1 - \left(1 - e^{-\frac{\mathcal{A} q_{\mathrm{SF}_i}}{\mathcal{P}p(d_{i0})}} \exp\left[-\frac{\gamma^2}{\cos\frac{\pi\alpha}{2}}\left(\frac{q_{SF_i}}{\mathcal{P}p(d_{i0})}\right)^{\alpha}\right] \mathcal{L}_{\mathcal{I}_0}\left(\frac{w}{\mathcal{P}p(d_{i0})}\right)\right) \times \exp\left(-2\pi\lambda_G \int_{d_{i0}}^{\infty} e^{-\frac{\mathcal{A} q_{\mathrm{SF}_i}}{\mathcal{P}p(x)}} \exp\left[-\frac{\gamma^2}{\cos\frac{\pi\alpha}{2}}\left(\frac{q_{SF_i}}{\mathcal{P}p(d_{ij})}\right)^{\alpha}\right] \mathcal{L}_{\mathcal{I}_j}\left(\frac{w}{\mathcal{P}p(x)}\right) x\,\mathrm{d}x\right). \quad (18)$$

until a value of 0.4 for $d_{i0} = 5$ km, and then reaches a value close to 0. Both this continuity and the value of 0 are mainly due to the densities of EDs for each SF. Indeed, in a sparse network, the densities λ_{E_k} are very small for $k \in [7; 11]$ (which leads to a small amount of co-SF interference for SF 7 to SF 11) and very big (i.e. close to λ_E) for SF 12 (which leads to a huge amount of interference). On the contrary, for a dense network, the density of EDs that are using SF 12 (i.e. $\lambda_{E_{12}}$) is much lower than in a sparse network. Thus, the number of co-SF interferers with SF 12 (i.e. for a distance between the ED and the GW greater than 5 km) is smaller, and then the SIR coverage probability is better than for a sparse network. Nevertheless, as the GWs are closer one to each other compared with a sparse network, the number of EDs that share the same SF (from SF 7 to SF 11) is higher, which leads to a worse SIR coverage probability for $d_{i0} \in [0, 5]$ km.

C. SUCCESS PROBABILITY

Figs. 8a and 8b show the success probability $H(\mathbf{e}_i)$ vs. the distance between the ED transmitter and its GW receiver with AWGN+α-stable noise with $\gamma = \gamma_1$ and $\gamma = \gamma_2$, respectively. The curves are taken from (18) for $\lambda_E = 5$ EDs per km^2 and $\lambda_G = 0.005, 0.01, 0.05$ GWs per km^2 (in blue, orange, green, yellow,purple and red, respectively). The solid and the dotted lines represent the success probability with AWGN noise only, and the success probability for AWGN noise + interferential α-stable noise, respectively.

As shown in Figs. 8a and 8b, the success probability is null for $d_{i0} > 5$ km in sparse and moderately dense networks. We have seen in the previous sections that for these GW deployments, the number of EDs using SF 12 is smaller than for other SFs. As the number of SF 12 EDs is very small, the integral taken into account in (18) is almost null.

For all the noises, the success probability follows curves with steps that correspond to the different SFs distances. This is due to both the SNR and SIR success probabilities explained in (11) and (16). Nevertheless, for an AWGN noise, the probability in a dense network is almost constant for low values of SFs, which is due to the fact that the number of EDs with low SFs is quite small compared to the ones in high SFs (and thus the SIR is high, as shown in Fig. 7).

With AWGN noise, the difference in success probability is becoming very high between dense and (moderately) sparse networks from SF 8. Indeed, the value of 0.8 is reached at $d_{i0} = 1.6$ km (SF 8) in (moderately) sparse networks, and at $d_{i0} = 6.2$ km for dense networks (SF 12). Such a difference denotes inevitably the need to increase the GW deployment density to reach a better success probability. Moreover, the maximum difference between dense and (moderately) sparse networks is reached at $d_{i0} = 5.1$ km, for a value of 0.93.

In Fig. 8a, we can see the effect of underlying IoT networks. Indeed, the addition of α-stable noise decreases the success probability in all the cases. This decrease is directly linked with the SNR success probability depicted in Fig. 6. For sparse and moderatly dense networks, the difference between LoRa-only network (i.e. with only AWGN) and LoRa+underlying IoT network is very thin for SFs 7, 8 and 12. However, for SFs 9 to 11, this difference is getting bigger, with a maximum difference of 0.06 for $d_{i0} = 3.95$ km in a sparse network, and 0.04 for $d_{i0} = 3.98$ km in a moderately dense network. Thus, we can say that the impact of underlying IoT networks on a sparse or moderately dense LoRa network is relatively weak in the case of a sub-urban environment (i.e. with $\gamma = \gamma_1$). On the contrary, in the case of an urban environment, i.e. with $\gamma = \gamma_2$, the impact of underlying networks is way bigger, as seen in Fig. 8b. Indeed, the success probability is reaching a value of 0.19 for $d_{i0} = 1.97$ km (SF 8) (whereas it reaches only 0.06 for the same d_{i0}). The maximum difference between AWGN and AWGN+α-stable noise is 0.24 for $d_{i0} = 2.9$ km (SF 9) in a sparse network, and 0.2 for the same value of d_{i0} in a moderately dense network. We can conclude that the addition of underlying IoT networks in an urban environment has a big impact on the success probability of a LoRa communication for a sparse or moderately dense GW deployment.

For a dense GW deployment, the main differences between AWGN and AWGN+α-stable noise are quite similar. In a sub-urban environment, the difference for SFs from 7 to 11 are quite thin. This difference reaches a value of 0.09 for $d_{i0} = 4.96$ km, which is acceptable. For SF 12 (recall that in a dense network, the number of EDs using SF 12 is very small), this difference reaches a value of 0.2 for $d_{i0} = 7.8$ km. Then, the addition of underlying IoT networks has a relatively big impact on the LoRa network for high SFs in this configuration. Nevertheless, as the number of EDs using high SFs is very negligible, we can say that *alpha*-stable noise impact is moderate. On the contrary, as shown in Fig. 8b, the impact of underlying IoT networks in an urban environment is big. Indeed, even for low SFs, the success probability decreases drastically (for SF8, at $d_{i0} = 1.9$ km, $\mathrm{H}(\mathbf{e}_i) = 0.98$ with AWGN noise, and $\mathrm{H}(\mathbf{e}_i) = 0.86$ with AWGN+α-stable noise). The difference beween the two values is even bigger for higher SFs, reaching a difference of 0.32 for $d_{i0} = 4.95$ km, i.e. for SF 11. For SF 12, the maximum difference is reached for $d_{i0} = 7$ km with a value of 0.5. However, as explained previously, the number of EDs using SF 12 is very small, and thus, even if this difference is high, the impact on the overall LoRa link success probability is quite moderate. We can conclude that in an urban environment, i.e. with $\gamma = \gamma_2$, the impact of underlying IoT networks on a LoRa link is severe in the case of a dense GW deployment. This impact is high for both high SFs (that are however seldom in use), and for low SFs.

Thus, we can conclude that underlying uncoordinated IoT networks have a big impact on the success probability of a LoRa communication for a sparse or a dense GW deployment and will undoubtedly have an effect on the overall LoRa coverage probability.

D. COVERAGE PROBABILITY

Fig. 9 shows the coverage probability $\mathcal{C}$ vs. density of GWs over density of EDs. The curves are taken from (8) for $\lambda_E = 5$

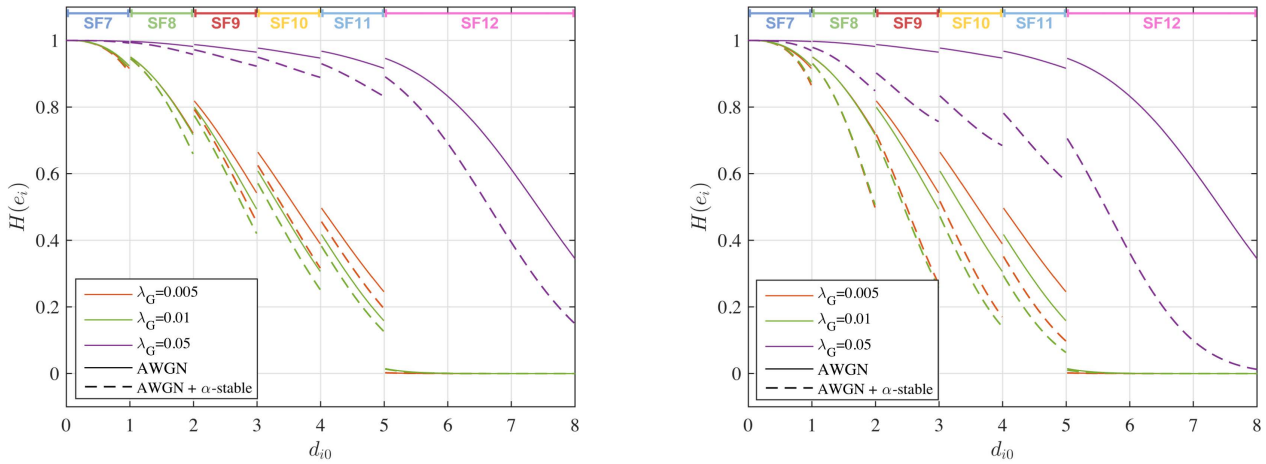

FIGURE 8. Success probability $H(e_i)$ vs. distance d_{i0} in km with γ_1 (a) and γ_2 (b). λ_G is given in GWs per km^2.

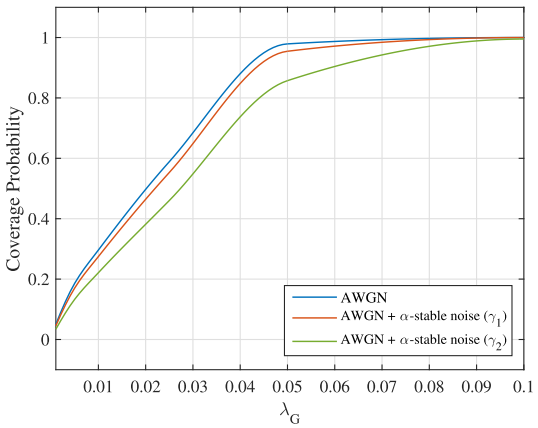

FIGURE 9. Coverage probability $\mathcal{C}$ vs. density of GWs (in GWs per km^2) for λ_E = 5 EDs per km^2. The first curve (AWGN) considers both LoRaWAN internal interference and AWGN noise. The other two curves (AWGN + α-stable noise γ_1 and γ_2) consider internal LoRaWAN network interference, AWGN noise and external interference (modeled by α-stable distributions) in the case of a moderate interference scenario (γ_1), and a dense interference scenario (γ_2). Note that external interference modeled by alpha-stable distributions does not affect SF allocation.

EDs per km^2. The blue, red and orange curves represent the coverage probabilities for AWGN noise only, AWGN + interferential α-stable noise with $\gamma = \gamma_1$ and AWGN + interferential α-stable noise with $\gamma = \gamma_2$, respectively.

We can see that for all the cases (AWGN and AWGN+α-stable noise), the coverage probability increases along the density of the gateways λ_G. The difference between the AWGN and AWGN+α-stable with γ_1 is quite thin for all the gateways deployment densities, with a maximum difference of 0.04. Note that the α-stable noise with γ_1 is quite small. Thus, we consider a small number of underlying IoT networks. Nevertheless, with a bigger α-stable noise (i.e. with γ_2), the difference is more significant. Indeed, a difference of 0.2 in the coverage probability is reached between the AWGN and the AWGN+α-stable noise. Moreover, the coverage probability reaches the value of 1 when $\lambda_G = 0.1$. Note that for this density, the number of EDs that use high SFs is very small. Thus, the integral in (8) takes into account almost only the very small values of d_{i0}. Indeed, when $\lambda_G = 0.1$, the density of GW is very high, as seen in Fig. 4. The calculation of the probability of coverage for a GW given by this equation is an integral which theoretically spreads over R+. However, the function $f_d(x)$ takes λ_G into consideration. This function involves a real integral that occupies only the GW's coverage radius. Thus, the d_{i0} integration variable is very small. These results show clearly that in an urban environment, i.e. in an area where the number of underlying IoT networks is high, the coverage probability is largely decreased.

Fig. 9 also shows that, for the considered conditions, the coverage probability reaches the value $\mathcal{C} = 0.95$ when $\lambda_G = 0.048$ for an environment without any underlying IoT network (i.e. with AWGN only). In an environment with a little amount of underlying IoT network (γ_1), this value of the coverage probability is reached for $\lambda_G = 0.071$. Finally, for a dense deployment of uncoordinated IoT networks (i.e. with AWGN and α-stable noise with γ_2), $\mathcal{C} = 0.95$ when $\lambda_G = 0.093$, which is almost twice as big as for the first studied case. In this specific scenario, we can conclude that in order to reach a decent coverage probability (i.e. $\mathcal{C} \geq 0.95$) in an urban environment with a big amount of underlying IoT networks, the density of the gateways must be almost doubled compared to an environment where there is no uncoordinated network.

V. CONCLUSION AND FUTURE WORKS

In this paper, we have introduced interfering underlying IoT networks in a LoRa network. The interfering networks have been modeled by α-stable distributions, and the coverage probability for various gateways densities has been calculated thanks to stochastic geometry-based analytic calculations. The theoretical calculations of the SNR, SIR, success probability and coverage probability for a LoRa link with

underlying unccordinated IoT networks is the main contribution of this work. Thanks to numerical analysis based on the theoretical results and on the implementation of a real path loss model that has been taken from in-situ measurements, we have proven that the presence of underlying networks surrounding a LoRa network could induce drastic decreases in the coverage probability of the overall studied network. The coverage probability decrease is particularly high for sparse and moderately dense LoRa networks (in terms of gateway deployment), with a maximum difference of 0.2 compared to a network with no neighboring network. All the observations in this work have led us to the conclusion that for an urban environment, i.e. in a space with a huge amount of surrounding uncoordinated IoT networks, the GW deployment should be doubled to reach a decent coverage probability. The challenge of communications of EDs with multiple GWs could increase the coverage probability. In future works, it could be interesting to study other spreading factor allocation strategies that consider the channel interference [45], that choose the least solicited spreading factors [46], or that use tools from matching theory to maximize the minimal short-term average user rates [47]. These strategies could possibly increase the coverage probability of the overall LoRa network. Another perspective could be linked with the density of end devices. Indeed, in this work, we have dealt with the coverage probability for a moderately dense end devices density. It could be interesting to analyze the coverage probability for sparse and very dense networks.

APPENDIX A
PROOF OF PROPOSITION 1

The success probability relative to the SIR corresponds to the probability that the ratio between the useful signal and the aggregated interference is greater than the value w. We consider that the studied i-th ED and j-th GW communicate via the SF k. Then, in (19), as shown at the bottom of the page, (a) comes from the definition of the SIR relative to the aggregated interference $\mathcal{I}_j$ at G_j. (b) comes from the fact that

$$
\begin{aligned}
\mathbb{P}[\mathrm{SIR}_{ij} \geq w] &\overset{(a)}{=} \mathbb{E}_{\mathcal{I}_j}\left[\mathbb{P}\left[|h_{ij}|^2 \geq \frac{w\mathcal{I}_j}{\mathcal{P}p(d_{ij})} \mid \mathcal{I}_j\right]\right] \\
&\overset{(b)}{=} \mathbb{E}_{\mathcal{I}_j}\left[e^{-\frac{w\mathcal{I}_j}{\mathcal{P}p(d_{ij})}}\right] \\
&\overset{(c)}{=} \mathbb{E}_{|h_{mj}|^2, d_{mj}}\left[e^{-\frac{w}{p(d_{ij})}\sum_{m>0}\Xi_{mk}|h_{mj}|^2 p(d_{mj})}\right] \\
&\overset{(d)}{=} \mathbb{E}_{d_{mj}}\left[\prod_{m\geq 1}\mathbb{E}_{|h_{mj}|^2}\left[e^{-w\Xi_{mk}|h_{mj}|^2\frac{d_{ij}^{\eta}}{d_{mj}^{\eta}}}\right]\right] \\
&\overset{(e)}{=} \mathbb{E}_{d_{mj}}\left[\prod_{m\geq 1}\frac{1}{1+w\Xi_{mk}\frac{d_{ij}^{\eta}}{d_{mj}^{\eta}}}\right] \\
&\overset{(f)}{=} \exp\left(-\int_{\mathbb{R}^2}\left(1-\frac{1}{1+w\frac{d_{ij}^{\eta}}{d_{mj}^{\eta}}}\right)2\pi\xi\lambda_{E_k}d_{mj}\mathrm{d}d_{mj}\right) \\
&\overset{(g)}{=} \exp\left(-2\pi w\xi\lambda_{E_k}\int_{l_{k-7}}^{+\infty}\left(\frac{\frac{d_{ij}^{\eta}}{d_{mj}^{\eta}}}{1+w\frac{d_{ij}^{\eta}}{d_{mj}^{\eta}}}\right)d_{mj}\mathrm{d}d_{mj}\right) \\
&\overset{(h)}{=} \exp\left(-\frac{2\pi w\ddot{\lambda}_{E_k}}{l_{k-7}^{\eta-2}(\eta-2)}\,{}_2F_1\left(1,1-\frac{2}{\eta},2-\frac{2}{\eta},-\frac{wd_{ij}}{l_{k-7}^{\eta}}\right)\right).
\end{aligned}
\tag{19}
$$

$$
\begin{aligned}
\mathrm{H}(d_{i0}) &\overset{(a)}{\geq} 1-\prod_j(1-\mathbb{P}[\mathrm{SNR}_{ij}\geq q_{\mathrm{SF}_i}]\mathbb{P}[\mathrm{SIR}_{ij}\geq w]) \\
&\overset{(b)}{\geq} 1-(1-\mathbb{P}[\mathrm{SNR}_{i0}\geq q_{\mathrm{SF}_i}]\mathbb{P}[\mathrm{SIR}_{i0}\geq w])\times\mathbb{E}_{d_{ij}}\left[\prod_{j\geq 1}(1-\mathbb{P}[\mathrm{SNR}_{ij}\geq q_{\mathrm{SF}_i}|d_{ij}]\mathbb{P}[\mathrm{SIR}_{ij}\geq w|d_{ij}])\right].
\end{aligned}
\tag{20}
$$

$h_{ij} \sim \text{Rayleigh}\left(\frac{1}{2}\right)$ and then $h_{ij}^2 \sim \text{Exp}(1)$. (c) is derived from the characterization of the interference. Note that Ξ_{mk} is a unit indicator, i.e. if the m-th ED uses the SF k, it equals 1, otherwise it is null. In other words, Ξ_{mk} indicates if the m-th ED is an interferer ($\Xi_{mk} = 1$) to the useful signal, or not ($\Xi_{mk} = 0$). It can also be noted that we take into account all the EDs in the whole infinite $\mathbb{R}^2$ space ($\sum_{m>0}$, as we consider that the useful link goes from the 0-th ED to the j-th GW). (d) comes from the fact that the channel fadings are assumed independent. We also take into account the fact that $\frac{p(d_{kj})}{p(d_{ij})} = \frac{d_{ij}^{\eta}}{d_{kj}^{\eta}}$. (e) comes from the fact that $\mathbb{E}_{|h|^2}\left[e^{-x|h|^2}\right] = \frac{1}{1+x}$. (f) comes from the probability generating functional of an inhomogeneous PPP. (g) comes from the change of the bounds of the integral. (h) is derived from the definition of the Gauss hypergeometric function. This last equality leads to (16) in Proposition 1.

APPENDIX B
PROOF OF PROPOSITION 2

The general success probability has been given in (7), and corresponds to the probability that a given E_i can be connected to any GW G_j:

$$\mathrm{H}(d_{ij}) = \mathbb{P}\left[\bigcup_j \{(\mathrm{SNR}_{ij} \geq q_{\mathrm{SF}_i}) \bigcap (\mathrm{SIR}_{ij} \geq w)\}\right].$$

Then, the success probability of the transmission for a given E_i that is connected to G_j is equal to the complement probability of this transmission not decoded by the other GWs:

$$\mathrm{H}(d_{ij}) = 1 - \mathbb{P}\left[\bigcap_j \overline{(\mathrm{SNR}_{ij} \geq q_{\mathrm{SF}_i}) \bigcap (\mathrm{SIR}_{ij} \geq w)}\right].$$

We assume that we take into account only the connections to the target GW G_0, then the success probability can be derived as given in (20), where (a) comes from the fact that we assume an independence between the SNR and the SIR for all the GWs and EDs, which leads to the lower bound inequality. In (b), we have decomposed the product in (a) with $j = 0$ and $j \geq 1$. The success probability given in (18) can be finally found after inserting the analytical values of the probabilities linked to the SNRs and the SIRs given in (11) and (16).

REFERENCES

[1] J. Parmar, T. Nagda, P. Palav, and H. Lopes, "IoT based weather intelligence," in *Proc. Int. Conf. Smart City Emerg. Technol. (ICSCET)*, Jan. 2018, pp. 1–4.
[2] A. Khan and A. Khachane, "Survey on IoT in waste management system," in *Proc. 2nd Int. Conf. (IoT Social, Mobile, Analytics Cloud) (I-SMAC)*, Aug. 2018, pp. 27–29.
[3] R. Du, P. Santi, M. Xiao, A. V. Vasilakos, and C. Fischione, "The sensable city: A survey on the deployment and management for smart city monitoring," *IEEE Commun. Surveys Tuts.*, vol. 21, no. 2, pp. 1533–1560, 2nd Quart. 2019.
[4] J. Eriksson, L. Girod, B. Hull, R. Newton, S. Madden, and H. Balakrishnan, "The pothole patrol: Using a mobile sensor network for road surface monitoring," in *Proc. 6th Int. Conf. Mobile Syst., Appl., Services*, 2008, pp. 29–39.
[5] Z. Li, Y. Zhu, H. Zhu, and M. Li, "Compressive sensing approach to urban traffic sensing," in *Proc. 31st Int. Conf. Distrib. Comput. Syst.*, Jun. 2011, pp. 889–898.
[6] S. Kim, S. Pakzad, D. Culler, J. Demmel, G. Fenves, S. Glaser, and M. Turon, "Wireless sensor networks for structural health monitoring," in *Proc. 4th Int. Conf. Embedded Networked Sensor Syst.*, 2006, pp. 427–428.
[7] N. Xu, S. Rangwala, K. K. Chintalapudi, D. Ganesan, A. Broad, R. Govindan, and D. Estrin, "A wireless sensor network for structural monitoring," in *Proc. 2nd Int. Conf. Embedded Networked Sensor Syst.*, 2004, pp. 13–24.
[8] D. A. Gandhi and M. Ghosal, "Intelligent healthcare using IoT: A extensive survey," in *Proc. 2nd Int. Conf. Inventive Commun. Comput. Technol. (ICICCT)*, Apr. 2018, pp. 800–802.
[9] Cisco. (2018). *Cisco Edge-to-Enterprise IoT Analytics for Electric Utilities*. [Online]. Available: https://www.cisco.com
[10] B. Mihajlov and M. Bogdanoski, "Overview and analysis of the performances of ZigBee-based wireless sensor networks," *Int. J. Comput. Appl.*, vol. 29, no. 12, pp. 28–35, Sep. 2011.
[11] P. M. L. An and T. Kim, "A study of the Z-wave protocol: Implementing your own smart home gateway," in *Proc. 3rd Int. Conf. Comput. Commun. Syst. (ICCCS)*, Apr. 2018, pp. 411–415.
[12] V. Baños-Gonzalez, M. S. Afaqui, E. Lopez-Aguilera, and E. Garcia-Villegas, "IEEE 802.11 ah: A technology to face the IoT challenge," *Sensors*, vol. 16, no. 11, p. 1960, 2016.
[13] N. Sornin and A. Yegin, "LoRaWAN 1.0. 3 specifications," *LoRa Alliance, Ver*, vol. 1, no. 3, pp. 1–72, 2018.
[14] A. Lavric, A. I. Petrariu, and V. Popa, "SigFox communication protocol: The new era of IoT?" in *Proc. Int. Conf. Sens. Instrum. IoT Era (ISSI)*, Aug. 2019, pp. 1–4.
[15] C. Goursaud and J. M. Gorce, "Dedicated networks for IoT: PHY/MAC state of the art and challenges," *EAI Endorsed Trans. Internet Things*, vol. 1, no. 1, Oct. 2015, Art. no. 150597.
[16] R. Chevillon, G. Andrieux, R. Négrier, and J.-F. Diouris, "Spectral and energy efficiency analysis of mmWave communications with channel inversion in outband D2D network," *IEEE Access*, vol. 6, pp. 72104–72116, 2018.
[17] B. Błaszczyszyn and P. Mühlethaler, "Analyzing LoRa long-range, low-power, wide-area networks using stochastic geometry," in *Proc. ACM Int. Conf. Proc. Ser.*, Mar. 2019, pp. 119–126.
[18] M. A. Ullah, J. Iqbal, A. Hoeller, R. D. Souza, and H. Alves, "K-means spreading factor allocation for large-scale LoRa networks," *Sensors*, vol. 19, no. 21, pp. 1–19, 2019.
[19] Z. Qin, Y. Liu, G. Y. Li, and J. A. McCann, "Performance analysis of clustered LoRa networks," *IEEE Trans. Veh. Technol.*, vol. 68, no. 8, pp. 7616–7629, Aug. 2019.
[20] N. Aftab, S. A. R. Zaidi, and D. McLernon, "Scalability analysis of multiple LoRa gateways using stochastic geometry," *Internet Things*, vol. 9, Mar. 2020, Art. no. 100132, doi: 10.1016/j.iot.2019.100132.
[21] T. H. Nguyen, W.-S. Jung, L. T. Tu, T. Van Chien, D. Yoo, and S. Ro, "Performance analysis and optimization of the coverage probability in dual hop LoRa networks with different fading channels," *IEEE Access*, vol. 8, pp. 107087–107102, 2020.
[22] A. Duda and M. Heusse, "Spatial issues in modeling LoRaWAN capacity," in *Proc. 22nd Int. ACM Conf. Model., Anal. Simul. Wireless Mobile Syst. (MSWIM)*, 2019, pp. 191–198.
[23] O. Georgiou and U. Raza, "Low power wide area network analysis: Can LoRa scale?" *IEEE Wireless Commun. Lett.*, vol. 6, no. 2, pp. 162–165, Apr. 2017.
[24] L.-T. Tu, A. Bradai, and Y. Pousset, "A new closed-form expression of the coverage probability for different QoS in LoRa networks," in *Proc. IEEE Int. Conf. Commun. (ICC)*, Jun. 2020, pp. 1–6.
[25] O. Georgiou, C. Psomas, and I. Krikidis, "Coverage scalability analysis of multi-cell LoRa networks," in *Proc. IEEE Int. Conf. Commun. (ICC)*, Jun. 2020, pp. 1–7.
[26] H. Linka, M. Rademacher, K. Jonas, and O. Aliu, "Path loss models for low-power wide-area networks: Experimental results using LoRa," in *Proc. VDE ITG-Fachbericht Mobilkommunikation*, Osnabrück, Germany, May 2018.
[27] P. Jorke, S. Bocker, F. Liedmann, and C. Wietfeld, "Urban channel models for smart city IoT-networks based on empirical measurements of LoRa-links at 433 and 868 MHz," in *Proc. IEEE 28th Annu. Int. Symp. Pers., Indoor, Mobile Radio Commun. (PIMRC)*, Oct. 2017, pp. 1–6.

[28] R. El Chall, S. Lahoud, and M. El Helou, "LoRaWAN network: Radio propagation models and performance evaluation in various environments in Lebanon," *IEEE Internet Things J.*, vol. 6, no. 2, pp. 2366–2378, Apr. 2019.
[29] G. Callebaut and L. Van der Perre, "Characterization of LoRa point-to-point path loss: Measurement campaigns and modeling considering censored data," *IEEE Internet Things J.*, vol. 7, no. 3, pp. 1910–1918, Mar. 2020.
[30] W. Xu, J. Y. Kim, W. Huang, S. S. Kanhere, S. K. Jha, and W. Hu, "Measurement, characterization, and modeling of LoRa technology in multifloor buildings," *IEEE Internet Things J.*, vol. 7, no. 1, pp. 298–310, Jan. 2020.
[31] C. Orfanidis, L. M. Feeney, M. Jacobsson, and P. Gunningberg, "Investigating interference between LoRa and IEEE 802.15.4g networks," in *Proc. IEEE 13th Int. Conf. Wireless Mobile Comput., Netw. Commun. (WiMob)*, Oct. 2017, pp. 1–8.
[32] A. Hoeller, R. D. Souza, H. Alves, O. L. Alcaraz Lopez, S. Montejo-Sanchez, and M. E. Pellenz, "Optimum LoRaWAN configuration under wi-SUN interference," *IEEE Access*, vol. 7, pp. 170936–170948, 2019.
[33] C. Zheng, M. Egan, L. Clavier, G. W. Peters, and J.-M. Gorce, "Copula-based interference models for IoT wireless networks," in *Proc. IEEE Int. Conf. Commun. (ICC)*, May 2019, pp. 1–6.
[34] L. Clavier, T. Pedersen, I. Larrad, M. Lauridsen, and M. Egan, "Experimental evidence for heavy tailed interference in the IoT," *IEEE Commun. Lett.*, vol. 25, no. 3, pp. 692–695, Mar. 2021.
[35] R. Chevillon, G. Andrieux, and J.-F. Diouris, "Coverage of LoRa links with a-stable modeled interfering underlying IoT networks," in *Proc. Joint Eur. Conf. Netw. Commun. 6G Summit (EuCNC/6G Summit)*, 2021, pp. 288–293.
[36] R. Chevillon, G. Andrieux, R. Négrier, and J.-F. Diouris, "Effects of directional antennas on outband D2D mmWave communications in heterogeneous networks," *AEU-Int. J. Electron. Commun.*, vol. 96, pp. 58–65, Nov. 2018.
[37] M. Haenggi, *Stochastic Geometry for Wireless Networks*. Cambridge, U.K.: Cambridge Univ. Press, 2012.
[38] M. Bor and U. Roedig, "LoRa transmission parameter selection," in *Proc. 13th Int. Conf. Distrib. Comput. Sensor Syst. (DCOSS)*, Jun. 2017, pp. 27–34.
[39] A. Grami, "Wireless communications," in *Introduction to Digital Communications*, A. Grami, Ed. Boston, MA, USA: Academic Press, 2016, Ch. 12, p. 493–527.
[40] C. C. Zheng, M. Egan, L. Clavier, G. W. Peters, and J.-M. Gorce, "On the validity of isotropic complex α-stable interference models for interference in the IoT," in *Proc. Colloque Francophone De Traitement Du Signal Et Des Images*, Lille, France, Aug. 2019, pp. 1–4. [Online]. Available: https://hal.archives-ouvertes.fr/hal-02263787
[41] P. C. Pinto and M. Z. Win, "Communication in a Poisson field of interferers—Part I: Interference distribution and error probability," *IEEE Trans. Wireless Commun.*, vol. 9, no. 7, pp. 2176–2186, Jul. 2010.
[42] R. Li, Z. Zhao, Y. Zhong, C. Qi, and H. Zhang, "The stochastic geometry analyses of cellular networks with α-stable self-similarity," *IEEE Trans. Commun.*, vol. 67, no. 3, pp. 2487–2503, Mar. 2019.
[43] D. Croce, M. Gucciardo, S. Mangione, G. Santaromita, and I. Tinnirello, "Impact of LoRa imperfect orthogonality: Analysis of link-level performance," *IEEE Commun. Lett.*, vol. 22, no. 4, pp. 796–799, Apr. 2018.
[44] A. Mahmood, E. G. Sisinni, L. Guntupalli, R. Rondón, S. A. Hassan, and M. Gidlund, "Scalability analysis of a LoRa network under imperfect orthogonality," *IEEE Trans. Ind. Informat.*, vol. 15, no. 3, pp. 1425–1436, Mar. 2019.
[45] A. Farhad, D.-H. Kim, and J.-Y. Pyun, "Resource allocation to massive Internet of Things in LoRaWANs," *Sensors*, vol. 20, no. 9, p. 2645, May 2020. [Online]. Available: https://www.mdpi.com/1424-8220/20/9/2645
[46] D.-T. Ta, K. Khawam, S. Lahoud, C. Adjih, and S. Martin, "LoRa-MAB: Toward an intelligent resource allocation approach for LoRaWAN," in *Proc. IEEE Global Commun. Conf. (GLOBECOM)*, Dec. 2019, pp. 1–6.
[47] L. Amichi, M. Kaneko, E. H. Fukuda, N. El Rachkidy, and A. Guitton, "Joint allocation strategies of power and spreading factors with imperfect orthogonality in LoRa networks," *IEEE Trans. Commun.*, vol. 68, no. 6, pp. 3750–3765, Jun. 2020.

ROMAIN CHEVILLON was born in La Roche-sur-Yon, France, in 1985. He received the Dipl.-Ing. degree in electronics and computer science from the Ecole Polytechnique de l'Université de Nantes (France), in 2008. He received the Ph.D. degree in electrical engineering from the University of Nantes, France, in 2018. He is currently an Assistant Professor at the Network and Telecommunications Department, University of Nantes. During his scholarship, he specialized in acoustics and advanced applied mathematics at the Technical University of Denmark in Kongens-Lyngby (Denmark). After spending three years in the music industry, he worked during four years as a Research Coordinator in the domains of music information retrieval (MIR) and cyber security. He integrated the Institut d'Électronique et des Technologies du numéRique (IETR), University of Nantes, in 2015 as a Ph.D. student. His research domains are mainly energy and spectral efficiencies in device-to-device communications and heterogeneous networks, and stochastic geometry.

GUILLAUME ANDRIEUX graduated in electrical engineering from Polytech Nantes and received the M.S. degree in telecommunications from the University of Nantes, France, in 2000. He received the Ph.D. degree in electrical engineering and the Habilitation à Diriger des Recherches degree from the University of Nantes, France, in 2004 and 2018, respectively. He is currently an Associate Professor at the Networks and Telecommunications Department, University of Nantes. His current research interests are digital communications, antenna processing, wireless sensor networks, energy efficiency in wireless networks, and channel estimation.

LAURENT CLAVIER (Senior Member, IEEE) received the Ph.D. degree in signal processing from TELECOM Bretagne (currently IMT Atlantique), Brest, France, in 1997, and the H.D.R. degree from Lille University, France, in 2009. Since October 2011, he has been a Professor with the Mines-Telecom Institute (IMT Lille Douai), the Institut d'Electronique, de Microélectronique et de Nanotechnologie (IEMN) (UMR CNRS 8520), and the Institut de Recherche sur les composants logiciels et matériels pour l'Information et la Communication Avancée (IRCICA) (USR CNRS 3380). His research interests include digital communications and the physical layer of wireless networks for the IoT, more specifically energy autonomous sensor networks and interference model and impact on ultradense wireless networks.

JEAN-FRANÇOIS DIOURIS received the Ph.D. degree from the University of Rennes I, France, in 1991. He is currently a Full Professor with Polytech Nantes, University of Nantes, France, and the Adjunct Director with the Institut d'Électronique et des Technologies du numéRique (IETR). His current research interests include digital communications, antenna processing, and energy efficient communications.